Dissipation in the superconducting mixed state in the presence of a small oscillatory magnetic-field component

M. P. Risse, M. G. Aikele, S. G. Doettinger, and R. P. Huebener
Physikalisches Institut, Lehrstuhl Experimentalphysik II, University of Tübingen, Morgenstelle 14, D-72076 Tübingen, Germany

C. C. Tsuei
IBM Thomas J. Watson Research Center, P. O. Box 218, Yorktown Heights, New York

M. Naito
NTT Basic Research Laboratories, 3-1 Morinosato-Wakamiya, Atsugi-shi, Kanagawa, 243-01, Japan
(Received 20 January 1997)

We have studied the electric resistivity in superconducting amorphous Mo_3Si films in a perpendicular magnetic field $B_0+B_1\ \sin\omega t$ with $B_1 \ll B_0$. For $B_1=0$ a resistive voltage only appeared due to flux creep above the critical current I_c. For $B_1>0$ we observed perfectly Ohmic behavior at currents $I \ll I_c$ $(B_1=0)$, with the resistivity increasing proportional to ω and B_1. We present a simplified model discussion explaining our results in terms of the magnetic flux transferred across the sample during each cycle of the oscillatory magnetic field because of the electric transport current. [S0163-1829(97)03222-0]

I. INTRODUCTION

The penetration of an ac magnetic field into an electrical conductor is limited by eddy current damping. The penetration depth reached during one cycle is referred to as the skin depth δ_0. In the mixed state of a type-II superconductor eddy current damping of magnetic-flux penetration takes place in the same way, except that the mixed-state electric conductivity now appears in the expression for δ_0. In the mixed state it is the Lorentz force of the shielding current, which drives the magnetic-flux lines into and out of the super-conductor.[1] For the geometry of a long slab oriented parallel to the dc and ac magnetic field we deal only with a one-dimensional problem and the discussion is relatively simple. However, for the geometry of a thin film in a perpendicular dc and ac field at least a two-dimensional treatment is needed. This geometry exhibits a number of special features of the magnetic and dissipative properties compared to the one-dimensional slab geometry.

Recently, interesting advances in the theory of the magnetic and dissipative properties of thin-film type-II superconductors in a perpendicular magnetic field have been reported.[2–7] Demagnetization effects due to the magnetic-flux expulsion from the sample and magnetic hysteresis require theoretical attention. Below the irreversibility line in the regime of flux creep the flux dynamics is complicated and results in a strongly nonlinear dependence of the electric field F upon the electric current density j. For an exact understanding of the magnetic and dissipative properties the underlying nonlinear and nonlocal diffusion equation for the space- and time-dependent electric field must be solved.

The magnetic response of a superconducting thin film in the mixed state to a perpendicular oscillatory magnetic field component is highly symmetric with flux entering and leaving the sample on opposite sides in the same way. This symmetry is broken if an electric transport current perpendicular to the magnetic-flux density is also applied. Because of this broken symmetry a dc electric field parallel to the current is expected. An exact theoretical treatment of this situation in the regime of flux creep has not yet been carried out, and the existing theories[2,7] must be extended to this case with broken symmetry.

Experiments where, in addition to a small oscillatory magnetic-field component, an electric transport current is also applied to the sample can be performed relatively easily. However, it appears that only a few such measurements have been reported in the past. These earlier measurements were carried out for superconducting Pb films in the intermediate state[8,9] and for Nb foils in the mixed state.[10] As their main result these experiments yielded the relaxation time τ for magnetic-flux penetration from the variation of the electric resistivity with the frequency of the oscillatory magnetic-field component.

In this paper we report measurements of the electric resistivity ρ appearing in thin-film type-II superconductors because of an applied electric transport current in the presence of a perpendicular magnetic field $B_0+B_1\ \sin\omega t$ with $B_1 \ll B_0$. We have restricted our measurements to the *low-frequency limit* $\omega\tau \ll 1$, where the frequency ω is much smaller than the inverse relaxation time τ^{-1} of magnetic-flux penetration. For the majority of our experiments we have used thin films of amorphous Mo_3Si. We also report some results of the electron-doped cuprate superconductor $Nd_{1.85}Ce_{0.15}CuO_x$.

In Sec. II we present a simplified model discussion, yielding the expected variation of the resistivity ρ with frequency ω and amplitude B_1 of the oscillatory magnetic field, and with the static field B_0 and the temperature. In Sec. III we describe the experimental procedures. Section IV contains the experimental results and their discussion, confirming the expected behavior outlined in Sec. II. Our conclusions are presented in Sec. V.

II. SIMPLIFIED MODEL DISCUSSION

An accurate theoretical treatment of the electric resistivity in the superconducting mixed state in the presence of an

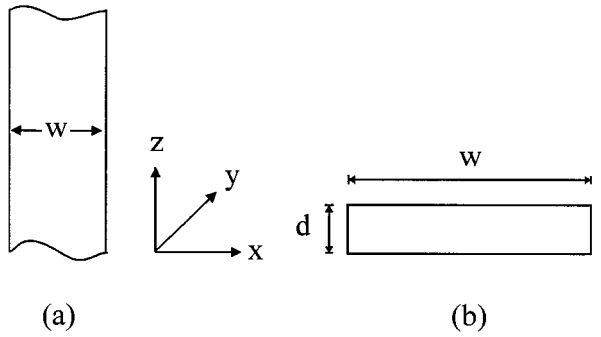

FIG. 1. (a) Slab geometry. (b) Thin-film geometry.

oscillatory magnetic-field component requires an extension of the existing theories[2,7] to the case where the symmetry is broken because of an applied transport current. In particular, the underlying nonlinear and nonlocal diffusion equation for the spatially and temporally varying electric field must be solved for this case. Instead of such a detailed theoretical treatment we present in the following a simplified model discussion, emphasizing the essential physics. We start with the one-dimensional geometry of a long slab oriented parallel to the applied magnetic field. Then we extend the results to the two-dimensional geometry of a thin film placed perpendicular to the magnetic field. In each case we restrict our discussion to the low-frequency limit $\omega\tau \ll 1$, where ω is the frequency of the magnetic-field oscillation and τ is the relaxation time for magnetic-flux penetration through the sample. Our geometries have also been discussed in Ref. 7.

A. Slab geometry

The slab geometry is schematically indicated in Fig. 1(a). The slab has infinite extension in the y and z directions and width w in the x direction. A magnetic field $B_0+B_1 \sin\omega t$ with $B_1 \ll B_0$ is applied along the z axis. An electric transport current with density j_{tr} is applied in the y direction.

In the absence of the transport current ($j_{tr}=0$), during each cycle of the field oscillation $B_1 \sin\omega t$ magnetic flux enters and leaves the slab symmetrically on both sides, and no net flux transfer across the slab in the x direction takes place. However, for $j_{tr} \neq 0$ during each cycle the Lorentz force of this current enhances the flux entry on one side of the slab and hinders the flux entry on the opposite side. Conversely, the sides where enhancement and hindrance occurs during flux exit, respectively, are exchanged. Hence, a net amount of flux is transferred across the slab in the x direction, and an electric field F is generated in the y direction. The fraction of the amplitude B_1 of the oscillatory flux density moving across the slab during each cycle depends upon the strength of flux pinning in the slab.

We assume in the following that flux motion in the sample shows the typical behavior characterized by the critical current density j_c: thermally activated flux flow for $j \ll j_c$, flux creep at $j \approx j_c$, and flux flow at $j \gg j_c$.[11] Here j_c is defined by a suitable electric field or voltage criterion. From the relation $j=(1/\mu_0)\mathrm{curl}\ B$ and the slab geometry we have $j_c=-1/\mu_0(\partial B_z/\partial x)_c$. During the oscillation of the applied magnetic field a large gradient of the vortex density builds up in the slab, since the value of the flux density in the sample lags behind the momentary value $B_0+B_1 \sin\omega t$ of the applied magnetic field at the sample edge. This flux density gradient propagates into and out of the sample. For illustration, we show in Fig. 2 a simplified case where the applied magnetic field is switched abruptly from B_0 to B_0+B_1 (a) and from B_0 to B_0-B_1(b). For simplicity, before each switch the flux density in the sample is assumed to be constant. The transport current is assumed to be zero. Upon each switch of the applied magnetic field, the large (positive or negative) flux density gradient propagates symmetrically at both sides into and out of the sample, respectively. At the end the critical flux density gradient corresponding to the critical current density $j_c=-1/\mu_0(\partial B_z/\partial x)_c$ is established across the sample. In the absence of a transport current, the vortex motion into and out of the sample is symmetric on both sides, and the total net flux transferred across the slab remains zero.

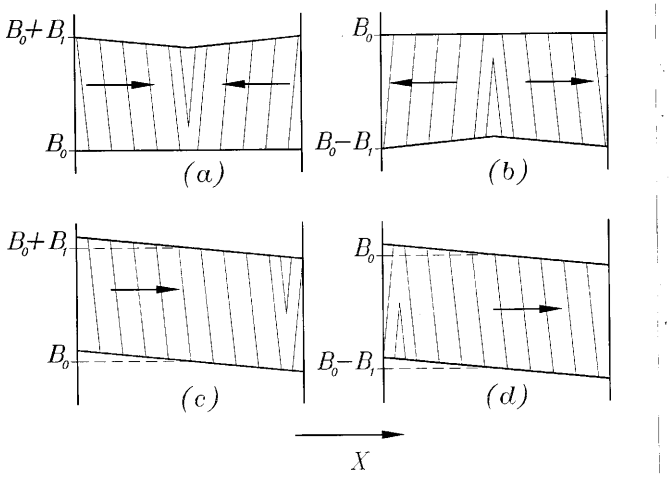

FIG. 2. Schematics of the flux entry and exit for the slab geometry if the applied magnetic field is abruptly increased [(a) and (c)] and decreased [(b) and (d)], respectively, by the amount B_1. (a) and (b) refer to zero transport current, (c) and (d) to the critical value of the transport current ($j_{tr}=j_c$). The arrows indicate the direction of the flux motion.

In the presence of an applied transport current this symmetry is broken, and a net flux transfer across the sample takes place during the sequence of an abrupt increase and decrease of the applied magnetic field. In Fig. 2, this is also illustrated for the case where the density of the transport current is equal to the critical current density, $j_{tr}=j_c$. Here, (c) and (d) refer to the switch from B_0 to B_0+B_1 and from B_0 to B_0-B_1, respectively. Following the switch upwards (c), the motion of the negative gradient $\partial B_z/\partial x$ to the right is much faster than the motion of the positive gradient $\partial B_z/\partial x$ to the left. After the switch downwards (d), the situation is opposite. As a result the sequence of both switches results in the net transfer of the total additional flux density B_1 across the sample. If the transport current density is smaller than the critical current density, $j_{tr}<j_c$, the transferred fraction of B_1 is approximately $(j_{tr}/j_c)B_1$.

These concepts can directly be extended to the case of the sinusoidal field modulation $B_0+B_1 \sin\omega t$. The vortex velocity associated with the flux transfer across the sample is $v_\varphi = w(\omega/2\pi)$. For the resulting electric field F we obtain

$$F = v_\varphi B_1 \frac{j_{tr}}{j_c} = w\frac{\omega}{2\pi} B_1 \frac{j_{tr}}{j_c}. \quad (1)$$

For the electric resistivity ρ we obtain

$$\rho = \frac{F}{j_{tr}} = w\frac{\omega}{2\pi}\frac{B_1}{j_c}. \quad (2)$$

We emphasize that the result of Eqs. (1) and (2) only apply in the low-frequency limit $\omega\tau \ll 1$, where the field oscillation $B_1 \sin\omega t$ completely penetrates the sample during each cycle. The magnetic relaxation time τ can be found from the skin depth $\delta_0 = (2\rho_c/\mu_0\omega)^{1/2}$ taking $\delta_0 = w/2$ and $\tau = \omega^{-1}$. Here ρ_c is the resistivity at the critical current density $j = j_c$. In this way we obtain

$$\tau = \mu_0(w^2/8\rho_c). \quad (3)$$

B. Thin-film geometry

The thin-film geometry is schematically shown in Fig. 1(b). The film of thickness d is parallel to the x-y plane, and the magnetic field $B_0 + B_1 \sin\omega t$ is applied in the z direction ($B_1 \ll B_0$). The width of the film in the x direction is w, and the length of the film in the y direction is infinite. An electric transport current with density j_{tr} is applied in the y direction.

For the thin-film geometry demagnetization effects are large, and the oscillatory magnetic-field component is strongly enhanced at the film edges. If one approximates the cross section of the film by a flat ellipsoid, the field at the edges is increased by the factor $(w/d+1)$.[12] If we take into account that during the penetration of the oscillatory magnetic-field component this field enhancement decreases linearly as the magnetic flux penetrates into the center of the film, we take $(w/2d+1)$ as the average enhancement factor. Hence, instead of Eq. (2), we now obtain for the resistivity

$$\rho = \frac{\omega}{2\pi}\frac{B_1 w}{j_c}\left(\frac{w}{2d}+1\right). \quad (4)$$

It has been pointed out, that approximating the cross section of the film by an exactly flat geometry rounded at both edges with a radius of curvature $d/2$ would be better than the shape of an ellipsoid.[5,7] In this case the enhancement factor of the field at the edges is $(\sqrt{w/d}+1)$. The average of this enhancement factor over the width of the film is approximated by $(\sqrt{w/2d}+1)$. Instead of Eq. (4) we then obtain

$$\rho = \frac{\omega}{2\pi}\frac{B_1 w}{j_c}\left(\sqrt{\frac{w}{2d}}+1\right). \quad (5)$$

For the thin-film geometry it is the second term in the relation $j_y = -1/\mu_0(\partial B_z/\partial x - \partial B_x/\partial z)$ which is important, and we have $j_y = (1/\mu_0)(\partial B_x/\partial z)$. Now the Lorentz force driving the vortices within the sample manifests itself through the curvature of the flux lines. However, in the presence of the oscillatory magnetic-field component flux moves into and out of the sample and gradients of the flux density develop in the x direction. Again, in the presence of a transport current in the y direction, the force acting on the vortices is increased in one direction and reduced in the opposite direction. In this way, a net transfer of magnetic flux across the sample appears resulting in the expressions for the resistivity in Eqs. (4) and (5).

The condition for the low-field limit $\omega\tau \ll 1$ must also be reevaluated for the thin-film geometry. Instead of Eq. (3) the relaxation time τ is now approximately given by

$$\tau = \mu_0 \frac{wd}{4\rho_c} \quad (6)$$

for the ellipsoidal cross section, and by

$$\tau = \mu_0 \frac{w\sqrt{2wd}}{8\rho_c} \quad (7)$$

for the flat cross section with rounded edges (we assume $w \gg d$).

According to Eqs. (4) and (5) the resistivity increases proportional to ω and B_1. The dependence of ρ on the static field B_0 and on the temperature is contained in the critical current density j_c. This behavior is well confirmed by our experiments described in Sec. IV. As we will see, our data also appear to favor the expression in Eq. (4) instead of that in Eq. (5).

III. EXPERIMENTAL PROCEDURES

A. Samples

Most of our experiments were performed with thin films of amorphous Mo_3Si which is an extreme type-II superconductor in the dirty limit with a Ginzburg-Landau parameter $\kappa \approx 60$.[13] The a-Mo_3Si films were deposited on single-crystalline MgO substrates. Their superconducting transition temperature was between 7.1 and 7.7 K and their electric resistivity ρ_n in the normal state slightly above T_c was about 200 $\mu\Omega$ cm. A typical resistive transition curve is shown in the inset of Fig. 4. a-Mo_3Si films display only very weak magnetic-flux pinning. Therefore, they are favorable for experimental studies of vortex dynamics. Details of the preparation and characterization of the a-Mo_3Si films are given elsewhere.[14]

We also carried out some measurements with epitaxial c-axis-oriented $Nd_{1.85}Ce_{0.15}CuO_x$ (NCCO) films prepared on $SrTiO_3$ substrates by means of conventional reactive coevaporation. We used two kinds of NCCO films: (a) Optimally doped films with the transition temperature $T_c = 23-24$ K and a resistivity of 50 $\mu\Omega$ cm slightly above T_c, and (b) films slightly overdoped with Ce with the transition temperature $T_c = 10-10.5$ K and a resistivity of about 20 $\mu\Omega$ cm slightly above T_c. Details of the preparation of our NCCO films can be found elsewhere.[15]

Our measurements were performed using a four-point sample geometry, fabricated by standard photolithography. The length between the voltage probes was always 200 μm, and the sample width was 20 or 40 μm. The film thickness was 50 or 100 nm for a-Mo_3Si and 100–120 nm for $Nd_{1.85}Ce_{0.15}CuO_x$.

B. Electric measurements

The substrate carrying the sample film was placed inside a cylindrical sample holder fabricated from teflon. A supercon-

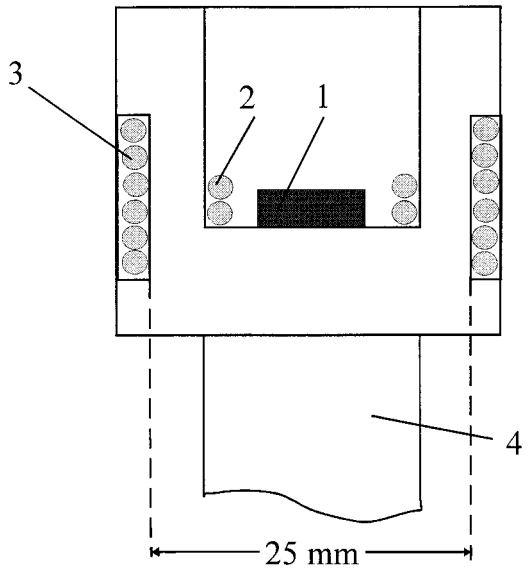

FIG. 3. Geometry of the sample and the high-frequency coils. (1) Substrate with sample film; (2) pick-up coil; (3) superconducting high-frequency coil; (4) teflon holer.

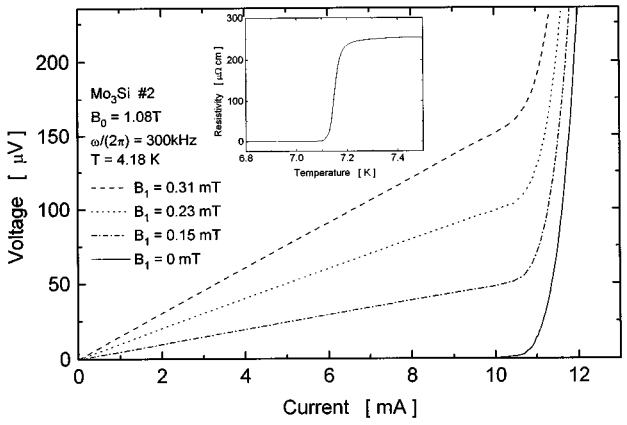

FIG. 4. Voltage versus current for an amorphous Mo_3Si film for different values of the amplitude B_1 of the oscillatory magnetic field, as indicated. $T=4.18$ K, $B_0=1.08$ T, $\omega/2\pi=300$ kHz, $w=40$ μm, $d=50$ nm.

ducting coil with 50 windings of 0.1 mm diameter NbTi wire was wound around the outside of the sample holder. The inner diameter and height of this coil was 25 and 7 mm, respectively. This coil served for applying an oscillatory magnetic field up to about 1 MHz frequency perpendicular to the sample film, which was placed close to the center of this coil. In order to monitor the amplitude of the oscillatory magnetic field, a pickup coil consisting of 5 windings of 0.1 mm diameter copper wire and surrounding the substrate area was located inside the high-frequency coil. This sample and coil configuration is shown schematically in Fig. 3. During the experiments it was inserted upside down into the center of a superconducting magnet generating a static magnetic field perpendicular to the sample film. The temperature range of our experiments was 4.2 K and below, and the arrangement shown in Fig. 3 was in direct contact with liquid He. The temperature was reduced below 4.2 K by pumping.

IV. EXPERIMENTAL RESULTS AND DISCUSSION

A. *a*-Mo_3Si

We have investigated three samples, all showing similar results. In Fig. 4 we show a typical voltage-current characteristic (VIC) for an *a*-Mo_3Si film at $B_0=1.08$ T and $T=4.18$ K. The influence of a small oscillatory magnetic field with amplitude B_1 of 0.15, 0.23, and 0.31 mT and frequency $\omega/2\pi=300$ kHz is also shown. In Fig. 4 only the low current range is displayed. Without the oscillatory magnetic field the VIC is highly nonlinear with a critical current of about 10.5 mA indicating the typical influence of flux pinning. On the other hand, in the presence of the oscillatory magnetic field we observe perfectly Ohmic behavior at low currents, with the voltage increasing proportional to the current. Apparently, at low currents the oscillatory magnetic field suppresses the influence of flux pinning on the VIC. At the critical current I_c where the voltage starts to rise rapidly with increasing current for $B_1=0$, a kink appears in all curves. This behavior for $I>I_c$ will be discussed below.

The feature of the upper three curves in Fig. 4 being straight lines passing through the origin with a well-defined slope allows us to express our results at low currents in terms of the electric resistivity $\rho=(V/I)(A/L)$. Here, A and L are the cross-sectional area and length of the sample film, respectively. In the presence of the oscillatory magnetic field $B_1 \sin\omega t$ this feature of perfectly Ohmic behavior of the VIC's at low currents has been observed in all our measurements for *a*-Mo_3Si. Therefore, in the following we present our results at low currents in terms of the resistivity ρ.

Figure 5 presents typical results on the dependence of the resistivity ρ upon the frequency $\omega/2\pi$ of the oscillatory magnetic field. In the frequency range shown the resistivity is seen to increase proportional to ω. The dependence of ρ upon the amplitude B_1 of the oscillatory field is shown in Fig. 6, indicating that ρ increases proportionally to B_1. A typical curve of ρ plotted versus the static field B_0 is presented in Fig. 7. The resistivity is seen to increase linearly with B_0, the

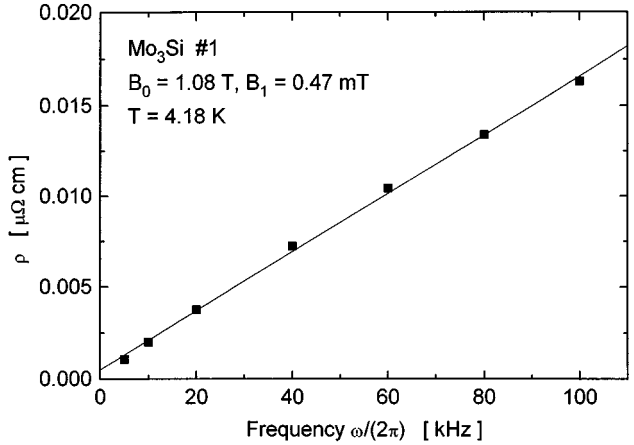

FIG. 5. Resistivity versus frequency of the oscillatory magnetic field. *a*-Mo_3Si, $T=4.18$ K, $B_0=1.08$ T, $B_1=0.47$ mT, $w=20$ μm, $d=100$ nm.

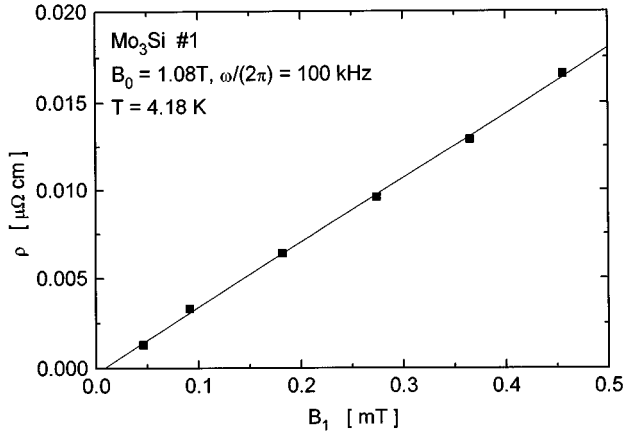

FIG. 6. Resistivity versus amplitude B_1 of the oscillatory magnetic field. a-Mo_3Si, $T=4.18$ K, $B_0=1.08$ T, $\omega/2\pi=100$ kHz, $w=20$ μm, $d=100$ nm.

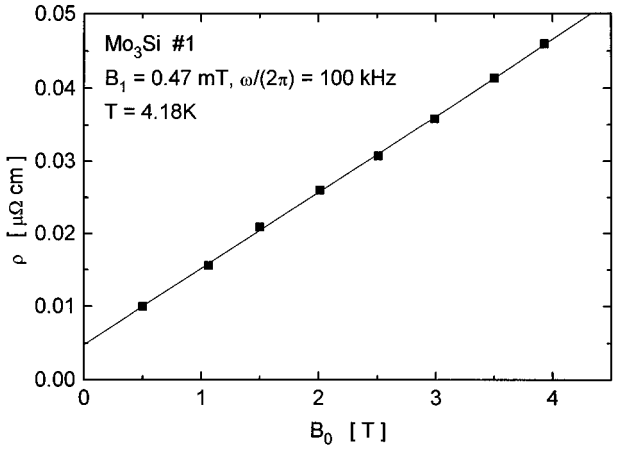

FIG. 7. Resistivity versus static magnetic field B_0. a-Mo_3Si, $T=4.18$ K, $B_1=0.47$ mT, $\omega/2\pi=100$ kHz, $w=20$ μm, $d=100$ nm.

straight line extrapolating to a finite value in the limit $B_0\rightarrow 0$. A typical curve of the temperature dependence of ρ is shown in Fig. 8.

Our results presented in Figs. 4–8 well confirmed the expressions for the resistivity in Eqs. (4) or (5) with the resistivity increasing proportional to ω and B_1. To check the validity of the low-frequency limit $\omega\tau\ll 1$ we estimate the relaxation time τ from Eq. (6). For this estimate we use the resistivity value ρ_c at the critical current density j_c with a 1μV voltage criterion. For $B_0=1.08$ T and 4.2 K we obtain $\tau=1.3\times 10^{-7}$ s, corresponding to the frequency $\omega=\tau^{-1}=7.7$ MHz. Hence, up to frequencies $\omega/2\pi$ of several hundred kHz we are well in the low-frequency limit.

In order to determine which of the two approximations for calculating the demagnetization effects is correct, we have calculated the quantity $C\equiv 2\pi\rho j_c/(wB_1\omega)$ for all our measurements. For a sample with $w=20$ μm and $d=100$ nm we obtained $C\approx 170$. From Eqs. (4) and (5) we expect $C=101$ and $C=11$, respectively. For another sample with $w=40$ μm and $d=50$ nm we found $C\approx 220$, compared to $C=400$ and $C=21$ expected from Eqs. (4) and (5), respectively. From this we conclude that Eq. (4) is closer to our experimental results than Eq. (5).

The variation of ρ with the static magnetic field B_0 and with temperature arises from the critical current density j_c in Eqs. (4) and (5). This has also been confirmed from an inspection of the product $\rho\, j_c$ for constant ω and B_1. This product remained constant within 10%.

As we can see from Fig. 4, the VIC's display a kink at the critical current I_c, where the voltage starts to rise rapidly with increasing current for $B_1=0$. We have pointed out in Sec. III that at this current value I_c the total amplitude B_1 of the oscillatory magnetic-field component is transferred across the sample during each cycle. For $I>I_c$ the voltage corresponding to this flux motion remains constant and is added to the voltage arising from flux creep associated with the static field B_0. Hence, during application of the oscillatory field we observe the parallel shift of the VIC's seen in Fig. 4 for $I>I_c$. Above the critical current I_c, such a parallel shift has always been found at constant B_0 and temperature for increasing values of ω or B_1. The steep rise of the VIC for $I>I_c$ results from flux creep as the dominating mechanism of vortex motion. For example, at the upper end of the VIC's displayed in Fig. 4 the sample resistivity is about 2.3×10^{-2} $\mu\Omega$ cm. This is by a factor of 10^4 lower than the normal-state resistivity $\rho_n=240$ $\mu\Omega$ cm for this specimen. On the other hand, $B_0=1.08$ T is about 10% of B_{c2}. Hence, flux flow as the resistive mechanism can be ruled out.

All our discussion in this section has been restricted to the low-frequency limit $\omega\tau\ll 1$. At the frequency $\omega=\tau^{-1}$ the resistivity is expected to reach a maximum and to decrease again at higher frequencies. This behavior has clearly been observed in the earlier experiments.[8–10] In the a-Mo_3Si films of our present study the high-frequency regime $\omega>\tau^{-1}$ could not be reached without experimental difficulties. Therefore, so far we have not taken any data in this high-frequency regime.

B. $Nd_{1.85}Ce_{0.15}CuO_x$

We have investigated four samples at 4.2 K. In the magnetic-field range $B_0=0.5$–1.5 T and for $B_1=0.47$ mT

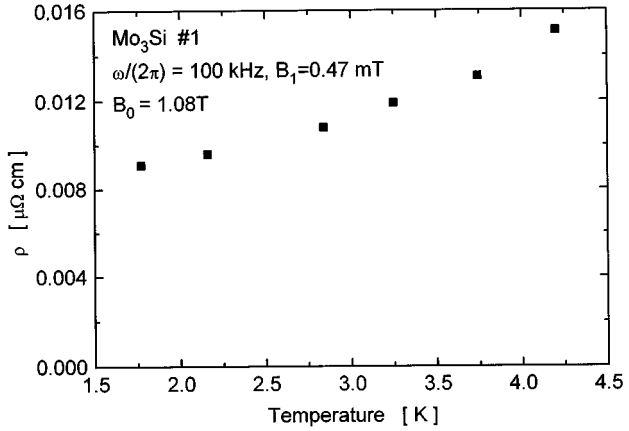

FIG. 8. Resistivity versus temperature. a-Mo_3Si, $T=4.18$ K, $B_1=0.47$ mT, $\omega/2\pi=100$ kHz, $w=20$ μm, $d=100$ nm.

and $\omega/2\pi=100$ kHz, the optimum doped NCCO films showed a reduction of the critical current only down to about 50% of its value in the absence of the oscillatory field ($B_1=0$). Apparently, at 4.2 K in these films the strength of flux pinning was relatively high. During each cycle of the oscillatory field the transfer of a finite fraction of the amplitude B_1 across the sample could be accomplished only for a transport current exceeding 50% or more of the critical current value I_c ($B_1=0$). On the other hand, in the magnetic field range $B_0=0.1-0.25$ T and for $B_1=0.47$ mT and $\omega/2\pi=300$ kHz the NCCO films slightly overdoped with Ce showed Ohmic behavior at low currents with the voltage increasing nearly proportional to the current, similar to the results for the a-Mo_3Si films discussed above.

V. CONCLUSIONS

In the superconducting mixed state the spatial symmetry of magnetic flux entry into the superconductor and flux exit out of the superconductor of a small oscillatory magnetic field $B_1 \sin\omega t$ is broken because of an electric transport current I_{tr} applied perpendicular to the field. As can be seen from a simplified model discussion, during each cycle of the oscillatory field a fraction of the amplitude B_1 is transferred across the sample, resulting in a resistive voltage. In the low-frequency limit $\omega\tau \ll 1$ this fraction is approximately given by the ratio I_{tr}/I_c, where I_c is the critical current in the absence of the oscillatory field ($B_1=0$). τ is the relaxation time for magnetic-flux penetration through the sample. In this low-frequency limit the electric resistivity increases proportional to ω and to B_1.

For demonstrating these effects a superconductor with a relatively low strength of flux pinning is favorable. We have performed experiments at 4.2 K and below with superconducting thin films of amorphous Mo_3Si, well confirming the results derived from a simplified model discussion. We have found similar effects also in thin films of the cuprate superconductor $Nd_{1.85}Ce_{0.15}CuO_x$, if the strength of flux pinning is reduced due to overdoping with Ce.

ACKNOWLEDGMENTS

Financial support of the Deutsche Forschungsgemeinschaft is gratefully acknowledged. The authors thank E. H. Brandt and N. Schopohl for helpful discussions, and D. Weischer for technical assistance.

[1] R. P. Huebener, *Magnetic Flux Structures in Superconductors* (Springer, Berlin, 1979).
[2] E. H. Brandt and A. Gurevich, Phys. Rev. Lett. **76**, 1723 (1996), and further references therein.
[3] A Gurevich and E. H. Brandt, Phys. Rev. Lett. **73**, 178 (1994).
[4] E. H. Brandt and M. Indenbom, Phys. Rev. B **48**, 12 893 (1993).
[5] M. Benkraouda and John R. Clem, Phys. Rev. B **53**, 5716 (1996).
[6] E. Zeldov *et al.*, Phys. Rev. Lett. **73**, 1428 (1994).
[7] E. Zeldov, John R. Clem. M. McElfresh, and M. Darwin, Phys. Rev. B **49**, 9802 (1994).
[8] R. P. Huebener, L. G. Stafford, and F. E. Aspen, Phys. Rev. B **5**, 3581 (1972).
[9] R. P. Huebener and V. A. Rowe, Physica **55**, 765 (1971).
[10] R. P. Huebener, G. Kostorz, and V. A. Rowe, J. Low Temp. Phys. **4**, 73 (1971).
[11] E. H. Brandt, Rep. Prog. Phys. **58**, 1465 (1995).
[12] R. P. Huebener, R. T. Kampwirth, and J. R. Clem, J. Low Temp. Phys. **6**, 275 (1972).
[13] A. W. Smith, T. W. Clinton, C. C. Tsuei, and C. J. Lobb, Phys. Rev. B **49**, 12 927 (1994).
[14] P. H. Kes and C. C. Tsuei, Phys. Rev. B **28**, 5126 (1983).
[15] M. Naito and H. Sato, Appl. Phys. Lett. **67**, 2557 (1995).